Control Theory and Technology (2024) 22:503–516
https://doi.org/10.1007/s11768-024-00221-x

RESEARCH ARTICLE

# On the optimality of uniform velocity–deceleration separation scheme for tethered satellite systems

Peng Yu[1,2] · Ji-Feng Zhang[3] · Shuping Tan[4] · Jin Guo[1,2] · Yanlong Zhao[3]

Received: 27 March 2023 / Revised: 4 July 2023 / Accepted: 23 November 2023 / Published online: 13 May 2024


**Abstract**
For mitigating the libration angle fluctuation of the tethered satellite system, this paper discusses how to make the uniform velocity–deceleration separation scheme achieve the best effect. First, a judgment condition is established to determine the tether state by comparing the tether length and the relative distance of the sub-satellite and the parent satellite. Based on the tethered satellite system dynamics equation and Clohessy–Wiltshire equation, dynamic models are given for four cases of tether states. Second, the influence of the uniform velocity–deceleration separation scheme on the libration angle is analyzed by taking the libration angle at the separation ending time and the mean absolute value of the libration angle as index functions. Then, the optimality problem of the uniform velocity–deceleration separation scheme is formulated as an optimization problem with constraints, and an approximate solution algorithm is given by combining the back propagation neural network and Newton–Raphson method of multiple initial values. Finally, the effectiveness of the proposed method is verified by a numerical simulation.

**Keywords** Tethered satellite systems · Libration angle · Uniform velocity–deceleration separation · Neural network

## 1 Introduction

As a kind of typical spacecraft, tethered satellites connect satellites to space shuttles, spacecraft or space stations via tethers or chains [1]. Compared with other spacecraft [2, 3], tethered satellites have the tether connection, which is convenient for delivering and recycling at any time [4–7]. Tethered satellites work at a distance of 100–150 km above the ground, and mainly perform tasks of collecting cosmic dust particles and observing the mechanism by which the sun affects climate or weather changes [8, 9]. In addition, if the tether is made of conductive materials, it not only can provide electricity for the satellites, but also can be used as the communication medium between the sub-satellite and the parent satellite [10]. Just because of these advantages, tethered satellites are widely used in the field of modern spaceflight.

The concept of tethered satellite originates from the idea of space elevator proposed by Tsiolkovsky in 1895 [11]. Limited by the aerospace and material technology, the idea was not been effectively carried out at that time. Until 1974, Ital-

This research was supported by the National Key R&D Program of China (2018YFA0703800), the National Natural Science Foundation of China (62173030) and the Beijing Natural Science Foundation (4222050).

✉ Jin Guo
guojin@ustb.edu.cn

Peng Yu
ustbyuu@163.com

Ji-Feng Zhang
jif@iss.ac.cn

Shuping Tan
sptan@amss.ac.cn

Yanlong Zhao
ylzhao@amss.ac.cn

[1] School of Automation and Electrical Engineering, University of Science and Technology Beijing, Beijing 100083, China

[2] Key Laboratory of Knowledge Automation for Industrial Processes, Ministry of Education, Beijing 100083, China

[3] Key Laboratory of Systems and Control, Academy of Mathematics and Systems Science, Chinese Academy of Sciences, Beijing 100190, China

[4] Beijing Institute of Control Engineering, Beijing 100094, China

ian astronomer Colombo formally proposed the concept of the tethered satellite system (TSS) [12]. In the 1990s, the electric tether system was designed and successfully applied to TSS-1 and TSS-1R jointly launched by Italian Space Agency and National Aeronautics and Space Administration [13]. In 1996, United States conducted the Tether Physics and Survivability experiment, the main purpose of which was to study the reliability and the long-term usability issues of space tethers. In the past 2 decades, the related field of TSS has developed rapidly, and a series of verification experiments have been implemented. In 2007, Russia and Europe jointly conducted the Young Engineer Satellite-2 test for verifying the feasibility of using the tether dynamic release method to realize the return of on-orbit loads. In 2010, Japan Aerospace Exploration Agency (JAXA) done the Tether Technologies Rocket experiment to study the feasibility of the isolated electrodynamic tether to collect ionospheric electrons and the orbital limit theory [14]. In 2017, JAXA tested the Kounotori Integrated Tether experiment to verify the space debris removal technology using the electrodynamic tether momentum exchange [15].

The TSS is usually modeled as the dumbbell model [16–20], which does not consider the quality, the toughness, the flexibility and the plasticity of the tether and ignores the attitude motion of satellites. The sub-satellite and the parent satellite are also regarded as two particles to obviously reflect the process of the tether deployment and retrieval. Cartmell and Mckenzie [16] illustrated that using the dumbbell model as the TSS model made it easier to study issues such as the tether control on elliptical orbits, the capturing spacecraft, the payload and the tether suspension rotation. Chen et al. [17] investigated the TSS dynamics model problem and found that the dumbbell model was one of the most important TSS models. Beletskii and Pivovarov [18] considered the modeling problem of the dumbbell-shaped satellite attitude and the motion equation under the multiple factors of gravity moment, aerodynamic pressure, aerodynamic friction and air gradient effect. Burov and Kosenko [19] discussed the dynamics of a variable length dumbbell in a central field of Newtonian attraction, where the dumbbell moved on an elliptical orbit similar to the Kepler orbit. Yu et al. [20] discussed the modeling and dynamics of a bare tape-shaped TSS under the atmospheric drag, the electrodynamic force and the heating impact.

The task of TSS mainly includes three phases: expansion phase, state maintenance phase and recovery phase. In order to suppress the fluctuation of the sub-satellite during deployment and recovery, a series of control methods have been developed, and the most commonly used one is based on the tension. Liu et al. [21] proposed a underactuated control scheme to handle the rotational deployment problem of a dual-body TSS. Chu et al. [22] put forward a hybrid tension control approach to stabilize the satellite system tethered to large space debris. Bourabah and Botta [23] designed a bang–bang length-rate control law and used the particle swarm algorithm to optimize the switching time and the tether length rate to reduce libration angles of the TSS. Su et al. [24] considered the controller with two robust terms for the triangular TSS formation with unmeasured velocities. Shan and Shi [25] gave a velocity-based detumbling strategy to effectively stabilize the TSS by controlling the movement of the tracker.

The separation scheme for the TSS mainly includes the rigid boom deployment, the momentum-exchange tether deployment, the electrodynamic tether deployment and the passive tether deployment. Among them, the momentum exchange tether deployment method is one of the most commonly used methods, since compared with traditional tether release ones, this can reduce the fluctuation and improve the stability of the TSS [16]. In this type of momentum-exchange tether deployment method, the uniform velocity–deceleration separation scheme (UVDSS) is one of the most important. This paper takes this as the research object, discusses how the separation scheme affects the libration angle, and explores how to design the separation scheme to minimize the fluctuation of the libration angle during the separation process of the TSS.

In practice, the UVDSS is often used to the separation of the sub-satellite and the parent satellite in the TSS. To mitigate the libration angle fluctuation, this paper discusses how to make the UVDSS achieve the best effect. The main contributions are briefed below:

- For determining the tether state, a judgment condition is introduced by comparing the tether length and the relative distance of the sub-satellite and the parent satellite. Based on the tethered satellite system dynamics equation and Clohessy–Wiltshire equation, dynamic models are given for four cases of tether states.
- A numerical calculation algorithm of the libration angle is proposed in stages of the uniform velocity separation and the deceleration separation. Taking the libration angle at the separation ending time and the mean absolute value of the libration angle as index functions, the influence of the UVDSS on the libration angle is analyzed.
- The optimality problem of the UVDSS is modeled as an optimization problem with constraints. Then, an approximate solution algorithm is given based on Newton–Raphson method of multiple initial values, where a back propagation (BP) neural network is used to model optimization objective functions.

The remainder of this paper is organized as follows. Section 2 sets up coordinate systems and dynamic equations associated with the TSS. Section 3 gives the UVDSS and analyzes its influences on the libration angle. And the optimality problem of such scheme is solved in Sect. 4. Section 5

employs a numerical example to demonstrate the results obtained. Section 6 gives the summary of this paper and looks forward to the future work.

## 2 Dynamics modeling of tethered satellite system (TSS)

### 2.1 Coordinate systems

Three coordinate systems are established to describe the TSS dynamics in the separation phase of the sub-satellite and the parent satellite, as shown in Fig. 1.

**1) Earth-centered coordinate system $O_eXYZ$**

The origin $O_e$ is located at the center of Earth. The axis $O_eX$ is along the intersection of the equatorial surface and the orbital surface, from the center of the earth to the ascending node. The axis $O_eZ$ is perpendicular to the orbital surface toward the arctic. The axis $O_eY$ is determined by the right-hand rule.

**2) Orbital coordinate system $Ox'y'z'$**

The origin $O$ is located at the centroid of the TSS. The axis $Oy'$ is along the direction of the systems orbital motion. The axis $Ox'$ is along the orbital radius vector $\overrightarrow{O_eO}$. The axis $Oz'$ is determined by the right-hand rule.

**3) Tethered coordinate system $OX_oY_oZ_o$**

The origin $O$ is located at the centroid of the TSS. The axis $OX_o$ is along the direction of the tether, and points from the parent satellite to the sub-satellite. The orbital coordinate system $Ox'y'z'$ is rotated by the angle $\theta$ along the axis $Oz'$ and the angle $\varphi$ along the axis $Oy'$, respectively, to obtain the tethered coordinate system $OX_oY_oZ_o$, where $\theta$ is the libration angle, and $\varphi$ is the spin angle.

### 2.2 TSS dynamics

In this paper, we concentrate on the change of the libration angle and ignore the spin angle. Let $\varphi = \dot{\varphi} = \ddot{\varphi} = 0$. Three control variables are considered during the entire process of the sub-satellite deployment: the tether length, the tether velocity and the libration angle. To facilitate the study, the following assumptions are given [26, 27].

- The TSS and the sun approximately form a two-body system. The centroid of the earth coincides with the center of the earth.
- The dumbbell model is used to describe the spatial position state of the TSS. That is, two satellites are regarded as the mass points, the tether mass and the flexural stiffness are not considered, and the tether length direction is rigid.
- Orbital perturbation forces such as the center body non-spherical perturbation force, the celestial gravity, the atmospheric resistance and the solar radiation pressure are not considered.

Affected by the gravitational field of Earth, the electromagnetic field and other factors, the tether velocity of the TSS and the relative velocity of the sub-satellite and the parent satellite are usually not synchronized. Therefore, the tether has two states: stretch and relaxation.

When the tether is in the stretch state, two satellites are constrained and seen as one system. Since the system is only affected by the gravitational force, it approximately satisfies the following dynamic equation [28, 29]:

$$\begin{cases} \ddot{l} - l\left[\left(\dot{\theta}+\Omega\right)^2 + \Omega^2\left(3\cos^2\theta - 1\right)\right] = -\dfrac{T}{\bar{m}}, \\ \ddot{\theta} + 2\left(\dot{\theta}+\Omega\right)\dfrac{\dot{l}}{l} + 3\Omega^2\sin\theta\cos\theta = 0, \end{cases} \tag{1}$$

where $l$, $\dot{l}$ and $\ddot{l}$ represent the tether length, the tether velocity and the tether acceleration at the current moment, respectively. $\theta$, $\dot{\theta}$ and $\ddot{\theta}$ represent the libration angle, the libration angle velocity and the libration angle acceleration at the current moment, respectively. $\Omega$ is the orbital angular velocity with $\Omega = \frac{2\pi}{T_{\text{run}}}$, where $T_{\text{run}}$ is the orbital period. $\bar{m} = m_1m_2/(m_1+m_2)$, where $m_1$ indicates the mass of the sub-satellite, $m_2$ indicates the mass of the parent satellite. $T$ means the tether tension.

When the tether is in the relaxation state, two satellites are seen as two independent systems. The orbital coordinate system is established with the parent satellite as the reference object satisfying the dynamic equation [30]:

$$\begin{cases} \ddot{x} - 2\omega\dot{y} - 3\omega^2 x = f_x, \\ \ddot{y} + 2\omega\dot{x} = f_y, \end{cases} \tag{2}$$

where $x$, $y$ are the projections of $\rho$ on the orbital coordinate system, $\rho$ represents the relative displacement of two satellites. $f_x$, $f_y$ are the components of the active perturbation

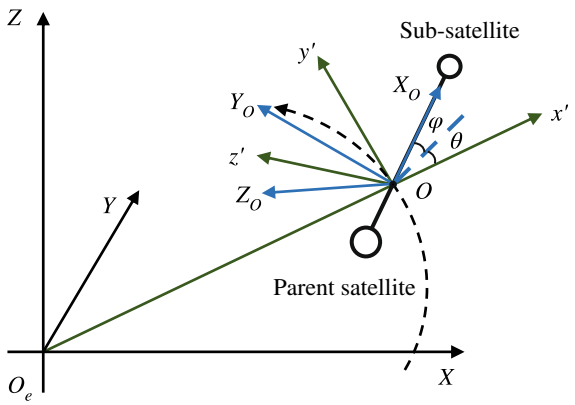


**Fig. 1** Coordinate systems

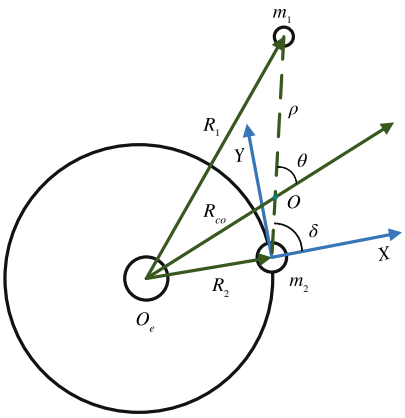


**Fig. 2** The relative motion of the sub-satellite and the parent satellite

force, respectively. $\omega$ is the orbital angular velocity of the parent satellite.

It can be known from the prerequisites that two satellites have no external force and $f_x = f_y = 0$. Then, by (2), we can get

$$\begin{cases} x = 2\left(2x_0 + \dfrac{\dot{y}_0}{\omega}\right) - \left(\dfrac{2\dot{y}_0}{\omega} + 3x_0\right)\cos(\omega t) \\ \quad + \left(\dfrac{\dot{x}_0}{\omega}\right)\sin(\omega t), \\ y = \left(y_0 - \dfrac{2\dot{x}_0}{\omega}\right) + 2\left(\dfrac{2\dot{y}_0}{\omega} + 3x_0\right)\sin(\omega t) \\ \quad + 2\left(\dfrac{\dot{x}_0}{\omega}\right)\cos(\omega t) - 3(\dot{y}_0 + 2\omega x_0)\, t, \end{cases} \tag{3}$$

where $x_0$, $y_0$, $\dot{x}_0$, $\dot{y}_0$ are the initial position and the initial velocity of the relative motion of two satellites. The relative motion of two satellites is shown in Fig. 2, where $R_1$, $R_{co}$ and $R_2$ are the orbital radii of the sub-satellite, the centroid of the TSS and the parent satellite, respectively.

Since the orbital radius of the TSS is much larger than the relative displacement between two satellites, we have $O_eO$ parallel to $O_em_2$. And based on the property of the corresponding angle, we get $\theta \approx \delta$ and $\omega \approx \Omega$. Letting $x = \rho\cos\delta = \rho\cos\theta$, $y = \rho\sin\delta = \rho\sin\theta$, and bringing them into (3), it follows that

$$\begin{cases} \rho\cos\theta = 2\left(2x_0 + \dfrac{\dot{y}_0}{\Omega}\right) - \left(\dfrac{2\dot{y}_0}{\Omega} + 3x_0\right)\cos(\Omega t) \\ \quad + \left(\dfrac{\dot{x}_0}{\Omega}\right)\sin(\Omega t), \\ \rho\sin\theta = \left(y_0 - \dfrac{2\dot{x}_0}{\Omega}\right) + 2\left(\dfrac{2\dot{y}_0}{\Omega} + 3x_0\right)\sin(\Omega t) \\ \quad + 2\left(\dfrac{\dot{x}_0}{\Omega}\right)\cos(\Omega t) - 3(\dot{y}_0 + 2\Omega x_0)\, t. \end{cases} \tag{4}$$

## 3 Uniform velocity–deceleration separation scheme (UVDSS) and its property

It can be seen from (1) and (4) that the solution of the libration angle is related to the tether velocity. For mitigating the libration angle fluctuation of the TSS, this section first gives the introduction of the uniform velocity–deceleration separation scheme (UVDSS) and then discusses how the tether velocity and the tethers release length in the uniform velocity separation phase affect the libration angle.

### 3.1 UVDSS and algorithm for obtaining the libration angle

Since the sub-satellite and the parent satellite are separated through the release of the tether, the UVDSS is making the tether keep a uniform velocity and then uniform deceleration until the tether reaches the tail end. The concrete process of releasing the tether can be seen in Fig. 3. For a UVDSS, the separation process of the TSS is divided into two phases. In the first phase, the tether is released at a uniform velocity, and in the second phase, the tether is released at a uniform deceleration. These two phases are called the uniform velocity separation phase and the deceleration separation phase, respectively.

Let the tether velocity and the tethers release length in the uniform velocity separation phase be $v$ and $\lambda$, respectively. Once $v$ and $\lambda$ are given in a UVDSS, the whole tether velocity can be obtained by the equation of motion. Thus, a given UVDSS can be represented by the two tuples $(v, \lambda)$.

From the relationship between velocity and displacement, it is known that the duration of the uniform velocity separation phase is $g_1(v, \lambda) = \frac{\lambda}{v}$, the duration of the deceleration separation phase is $g_2(v, \lambda) = \frac{2}{v}(L - \lambda)$, and the total separation time of the TSS is

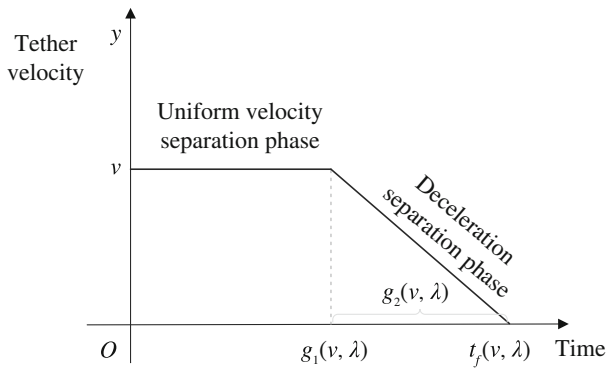


**Fig. 3** The tether velocity in a UVDSS

$$t_f(v,\lambda) = g_1(v,\lambda) + g_2(v,\lambda) = \frac{1}{v}(2L-\lambda). \tag{5}$$

Next, we discuss the TSS dynamic equations for the uniform velocity separation phase and the deceleration separation phase, respectively. The comparison of the tether length and the relative distance of the sub-satellite and the parent satellite can be used as a judgment condition to determine whether the tether is in a relaxation state or in a stretch state. Then, according to the tether state, the TSS has the different dynamic equation. Letting the initial relative velocity of the sub-satellite and the parent satellite be $v_0$, their relative distance $\rho$ can be obtained in light of (4).

**1) Uniform velocity separation phase: $0 \le t \le g_1(v,\lambda)$**

In this phase, it is known that $l = vt$, $\dot{l} = v$ and $\ddot{l} = 0$.

If $\rho \le l$, then the tether is in a relaxation state, and the TSS is regarded as two relative motion systems. The dynamic equation is given by (4).

If $\rho > l$, then the tether is in a stretch state, and the TSS is viewed as one system. By (1), the dynamic equation is

$$\begin{cases} vt\left[\left(\dot{\theta}+\Omega\right)^2 + \Omega^2\left(3\cos^2\theta - 1\right)\right] = \dfrac{T}{\bar{m}}, \\ \ddot{\theta} + \dfrac{2\left(\dot{\theta}+\Omega\right)}{t} + 3\Omega^2\sin\theta\cos\theta = 0. \end{cases} \tag{6}$$

**2) Deceleration separation phase: $g_1(v,\lambda) \le t \le t_f(v,\lambda)$**

For this phase, the tether initial velocity is $v$, the final velocity is 0 and the tether's total release length is $L-\lambda$. Thus, it is known that

$$\begin{cases} l = \lambda + v\left(t - g_1(v,\lambda)\right) - \dfrac{v^2\left(t-g_1(v,\lambda)\right)^2}{4(L-\lambda)}, \\ \dot{l} = v - \dfrac{v^2\left(t-g_1(v,\lambda)\right)}{2(L-\lambda)}, \\ \ddot{l} = -\dfrac{v^2}{2(L-\lambda)}. \end{cases} \tag{7}$$

If $\rho \le l$, then the tether is in a relaxation state, and the dynamic equation is given by (4).

If $\rho > l$, then the tether is in a stretch state, by (1) and (7) the dynamic equation is given by (8).

In view of dynamic equations in the two phases, we know that when the tether is in a relaxation state, the libration angle $\theta$ follows (4), which yields (9).

$$\begin{cases} \dfrac{v^2}{2(L-\lambda)} + \left(\lambda + v\left(t-g_1(v,\lambda)\right) - \dfrac{v^2\left(t-g_1(v,\lambda)\right)^2}{4(L-\lambda)}\right)\left[\left(\dot{\theta}+\Omega\right)^2 + \Omega^2\left(3\cos^2\theta - 1\right)\right] = \dfrac{T}{\bar{m}}, \\ \ddot{\theta} + \dfrac{-8v\lambda + 8vL - 4v^2\left(t-g_1(v,\lambda)\right)}{-4\lambda^2 + \left(4L - 4v\left(t-g_1(v,\lambda)\right)\right)\lambda + 4v\left(t-g_1(v,\lambda)\right)L - v^2\left(t-g_1(v,\lambda)\right)^2}\left(\dot{\theta}+\Omega\right) \\ \quad + 3\Omega^2\sin\theta\cos\theta = 0. \end{cases} \tag{8}$$

$$\theta = \arctan\left(\frac{2\left(2x_0 + \frac{\dot{y}_0}{\Omega}\right) - \left(\frac{2\dot{y}_0}{\Omega} + 3x_0\right)\cos(\Omega t) + \left(\frac{\dot{x}_0}{\Omega}\right)\sin(\Omega t)}{y_0 - \frac{2\dot{x}_0}{\Omega} + 2\left(\frac{2\dot{y}_0}{\Omega} + 3x_0\right)\sin(\Omega t) + 2\frac{\dot{x}_0}{\Omega}\cos(\Omega t) - 3\left(\dot{y}_0 + 2\Omega x_0\right)t}\right). \tag{9}$$

When the tether is in a stretch state, $\theta$ follows second-order nonlinear differential equations (6) and (8). At this point, there is no displayed solution of $\theta$ and then we can use the 4-order Runge–Kutta method to get a numerical solution of $\theta$.

In summary, the comparison of two phases is shown in Table 1, and the algorithm for obtaining the libration angle $\theta$ is shown in Algorithm 1.

**Algorithm 1** Algorithm for obtaining the libration angle $\theta$

1: Give the total tether length $L$, the orbital angular velocity $\Omega$, the mass of the sub-satellite $m_1$, the mass of the parent satellite $m_2$, the initial relative velocity $v_0$ and a UVDSS $(v,\lambda)$.
2: **for** $t = 0 : g_1(v,\lambda)$
3: solve (4) to obtain $\rho$, and $l = vt$.
4: **if** $\rho \le l$
5: solve (9) to obtain $\theta$, and $T = 0$.
6: **else if**
7: solve (6) to obtain $\theta$ with the 4-order Runge–Kutta method, and then obtain $T$ based on $\theta$ and (6).
8: **end if**
9: **end for**
10: **for** $t = g_1(v,\lambda) : t_f(v,\lambda)$
11: solve (4) to obtain $\rho$, and solve (7) to obtain $l$.
12: **if** $\rho \le l$
13: solve (9) to obtain $\theta$, and $T = 0$.
14: **else if**
15: solve (8) to obtain $\theta$ with the 4-order Runge–Kutta method, and then obtain $T$ based on $\theta$ and (8).
16: **end if**
17: **end for**

Algorithm 1 is done by calling two models (the TSS dynamic model and the Clohessy–Wiltshire equation) and the 4-order Runge–Kutta algorithm. Thus, the convergence of Algorithm 1 is principally determined by the 4-order Runge–Kutta algorithm, whose convergence is mainly ensured by the Lipschitz condition [31, 32].

**Table 1** Comparison of two phases

| | Uniform velocity separation phase | Deceleration separation phase |
|---|---|---|
| The tether length $l$ | Monotonically increasing | Parabola |
| The tether velocity $v$ | Constant | Monotonically decreasing |
| The duration | $g_1(v, \lambda)$ | $g_2(v, \lambda)$ |
| The dynamic equation | (6) or (4) | (8) or (4) |

Let $f(\theta, \dot{\theta}) = -2\left(\dot{\theta} + \Omega\right)\frac{\dot{l}}{l} - 3\Omega^2 \sin\theta\cos\theta$ based on (1). Then, we have

$$\frac{\partial f(\theta, \dot{\theta})}{\partial \theta} = -3\Omega^2\cos^2\theta + 3\Omega^2\sin^2\theta, \quad \frac{\partial f(\theta, \dot{\theta})}{\partial \dot{\theta}} = -2\frac{\dot{l}}{l}.$$

It can be seen that $\frac{\partial f(\theta,\dot{\theta})}{\partial \theta}$ and $\frac{\partial f(\theta,\dot{\theta})}{\partial \dot{\theta}}$ are continuous over the domain. And for any $\theta_1$, $\dot{\theta}_1$, $\theta_2$ and $\dot{\theta}_2$, it follows that

$$\begin{aligned}
&\left|f\left(\theta_1, \dot{\theta}_1\right) - f\left(\theta_2, \dot{\theta}_2\right)\right| \\
&= \Big| -2\left(\dot{\theta}_1 + \Omega\right)\frac{\dot{l}}{l} - 3\Omega^2 \sin\theta_1\cos\theta_1 \\
&\quad +2\left(\dot{\theta}_2 + \Omega\right)\frac{\dot{l}}{l} - 3\Omega^2 \sin\theta_2\cos\theta_2\Big| \\
&\le \left|2\left(\dot{\theta}_2 + \Omega\right)\frac{\dot{l}}{l} - 2\left(\dot{\theta}_1 + \Omega\right)\frac{\dot{l}}{l}\right| \\
&\quad +\left| -3\Omega^2 \sin\theta_1\cos\theta_1 - 3\Omega^2 \sin\theta_2\cos\theta_2\right| \\
&\le 2\frac{\dot{l}}{l}\left|\dot{\theta}_1 - \dot{\theta}_2\right| + \frac{3}{2}\Omega^2\left|\sin\left(2\theta_1\right) - \sin\left(2\theta_2\right)\right| \\
&\le 2\frac{\dot{l}}{l}\left|\dot{\theta}_1 - \dot{\theta}_2\right| + 3\Omega^2\left|\theta_1 - \theta_2\right|.
\end{aligned}$$

In views of the definition of Lipschitz condition, it can be seen that $f(\theta, \dot{\theta})$ satisfies the Lipschitz condition. This lays the foundation for the convergence of Algorithm 1.

### 3.2 Effect of the tether velocity in UVDSS on the libration angle

The libration angle $\theta$ is a function of the time $t$ and is affected by $v$ and $\lambda$. For this, it is written as $\theta = \theta(t; v, \lambda)$, where $t \in \left[0, t_f(v, \lambda)\right]$. Define the mean absolute value of the libration angle as

$$|\theta|_{\text{ave}}(v, \lambda) = \frac{1}{t_f(v, \lambda)}\int_0^{t_f(v,\lambda)} |\theta(t; v, \lambda)|\,\mathrm{d}t, \tag{10}$$

where $t_f(v, \lambda)$ is given by (5).

The libration angle at the separation ending time and the mean absolute value of the libration angle are adopted as index functions to analyze the influence of the tether velocity on the libration angle. For a given tether's release length in the uniform velocity separation phase, denote

**Table 2** System parameters

| Physical quantity | Value |
|---|---|
| The mass of the sub-satellite | $m_1 = 40\,\text{kg}$ |
| The mass of the parent satellite | $m_2 = 200\,\text{kg}$ |
| The total tether length | $L = 800\,\text{m}$ |
| The orbital height | $h = 500\,\text{km}$ |
| The initial separation velocity | $v_0 = 0.3\,\text{m/s}$ |

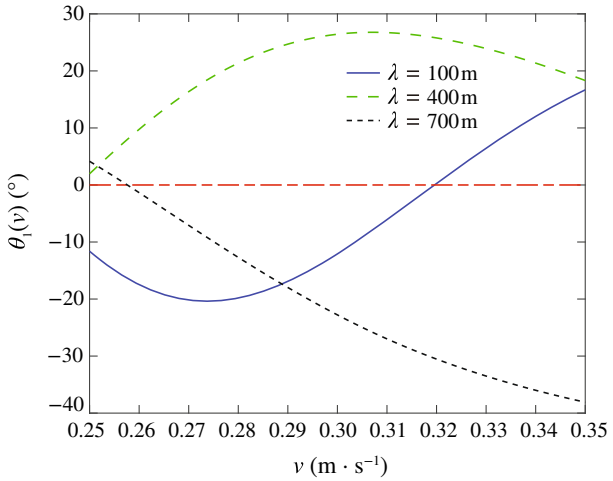


**Fig. 4** The function curve of $\theta_1(v)$ with respect to $v$ for a given $\lambda$

$$\theta_1(v) = \theta\left(t_f; v, \lambda\right),$$
$$\theta_2(v) = |\theta|_{\text{ave}}(v, \lambda).$$

Next, we use simulations to show the effect of the tether velocity on $\theta_1(v)$ and $\theta_2(v)$. System parameters are given by Table 2. Choose $\lambda = 100\,\text{m}$, $400\,\text{m}$ and $700\,\text{m}$, respectively. The relationships between $\theta_1(v)$, $\theta_2(v)$ and $v$ are shown in Figs. 4 and 5 according to Algorithm 1.

From Figs. 4 and 5, one can see that the relationship between $\theta_1(v)$, $\theta_2(v)$ and $v$ is closely related to the value of $\lambda$. The value of $\lambda$ determines the properties of such relationships, such as the convexity, the monotone interval, the existence of zero point, etc.

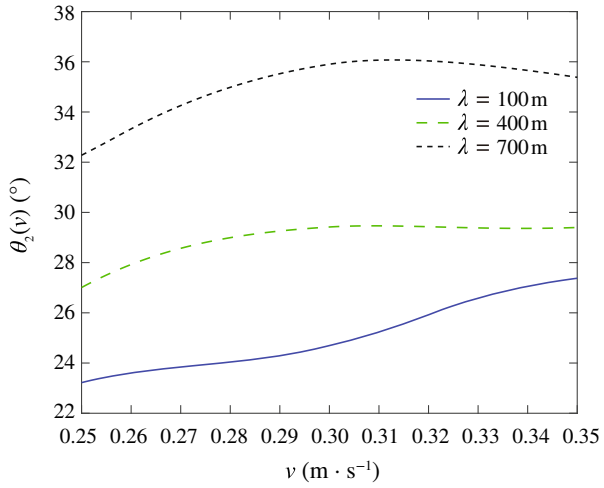


**Fig. 5** The function curve of $\theta_2(v)$ with respect to $v$ for a given $\lambda$

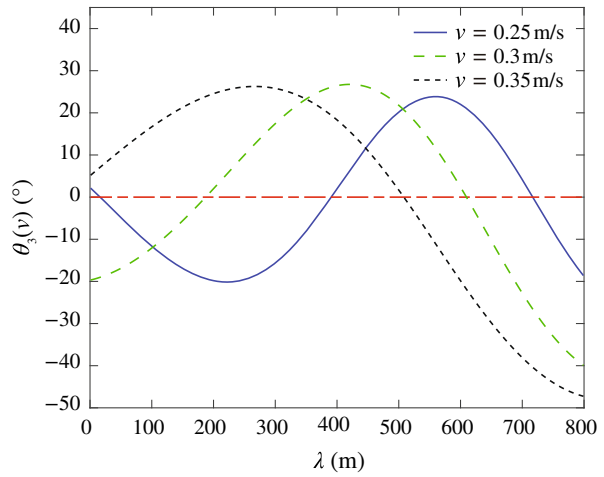


**Fig. 6** The function curve of $\theta_3(\lambda)$ with respect to $\lambda$ for a given $v$

### 3.3 Effect of the tether's release length in the uniform velocity separation phase on the libration angle

We discuss the influence of $\lambda$ on the libration angle at the separation ending time and the mean absolute value of the libration angle by simulations. For this, $v$ is given and we denote

$$\theta_3(\lambda) = \theta\left(t_f; v, \lambda\right),$$
$$\theta_4(\lambda) = |\theta|_{\text{ave}}(v, \lambda).$$

The parameters of the TSS are selected as shown in Table 2. Let $v = 0.25\,\text{m/s}, 0.3\,\text{m/s}, 0.35\,\text{m/s}$, respectively. Algorithm 1 is used to get $\theta$, and index functions $\theta_3(\lambda)$ and $\theta_4(\lambda)$ are analyzed with respect to $\lambda$, respectively. The simulation results are shown in Figs. 6 and 7.

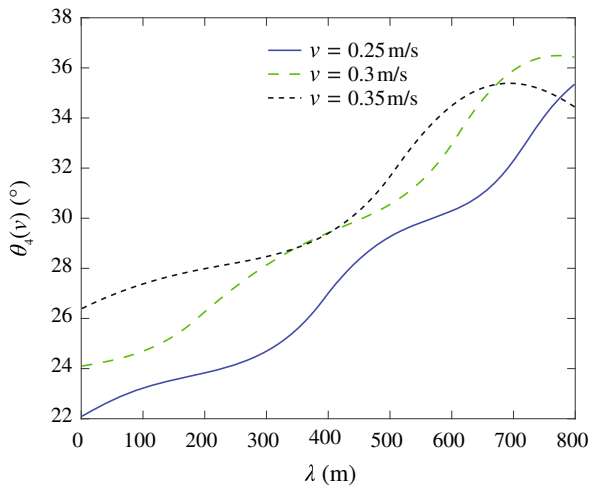


**Fig. 7** The function curve of $\theta_4(\lambda)$ with respect to $\lambda$ for a given $v$

It can be seen from Fig. 6 that $\theta_3(\lambda)$ is nonlinearly related to $\lambda$. There is at least one zero point for $\theta_3(\lambda)$, that is, there is at least a UVDSS to guarantee that the libration angle at the separation ending time is 0. If there exist multiple zero points, it is necessary to consider comprehensively Fig. 7 for the further judgment. For example, there are three zero points when $v = 0.25\,\text{m/s}$, including $\lambda = 16\,\text{m}, 390\,\text{m}, 716\,\text{m}$. Since $\theta_4(\lambda)$ is monotonically increasing with respect to $\lambda$ in Fig. 7, it can be seen that the separation scheme with $v = 0.25\,\text{m/s}$, $\lambda = 16\,\text{m}$ is the best one.

***Remark 1*** It can be seen from Sects. 3.2 and 3.3 that any change in $v$ and $\lambda$ will affect the change of the libration angle of the whole process, and $(v, \lambda)$ has no linear relationship with $\theta_{t_f}(v, \lambda)$ and $|\theta|_{\text{ave}}(v, \lambda)$, respectively. Therefore, it is necessary to fit $\theta_{t_f}(v, \lambda)$ and $|\theta|_{\text{ave}}(v, \lambda)$ based on the data-based algorithm.

## 4 Optimality of the UVDSS and solution algorithm

This section discusses how to select $v$ and $\lambda$ to make the separation process of the sub-satellite and the parent satellite as stable as possible, that is, how to select $v$ and $\lambda$ to optimize the libration angle at the separation ending time and the mean absolute value of the libration angle.

### 4.1 Modeling of the optimality problem of the UVDSS

Denote the libration angle at the separation ending time as $\theta_{t_f}(v, \lambda)$, i.e.,

$$\theta\left(t_f; v, \lambda\right) = \theta(\frac{1}{v}(2L - \lambda); v, \lambda) := \theta_{t_f}(v, \lambda). \tag{11}$$

A solution of $\theta_{t_f}(v,\lambda)=0$ gives a UVDSS that makes the librational angle be at the equilibrium, that is, the stability of the TSS is guaranteed. In view of (10), it can be seen that $|\theta|_{\text{ave}}(v,\lambda)$ represents the libration degree of the sub-satellite and the parent satellite during the release process for a given UVDSS.

Based on the above considerations, $|\theta|_{\text{ave}}(v,\lambda)$ is used as the index function, $\theta_{t_f}(v,\lambda)=0$ is used as a constraint condition, the optimality problem of the UVDSS is established as

$$\min_{(v,\lambda)} \{|\theta|_{\text{ave}}(v,\lambda)\} \tag{12}$$

$$\text{s.t. } \theta_{t_f}(v,\lambda)=0, \tag{13}$$

$$v\in[\underline{v},\overline{v}],\quad \lambda\in(0,L), \tag{14}$$

where $\underline{v}$ and $\overline{v}$ represent the lower bound and the upper bound of the tether velocity respectively. The solution of the optimization problem above is denoted as $(v^*,\lambda^*)$, called the optimal UVDSS.

***Remark 2*** 1) The optimization goal (12) is the mean value of the full-period libration angle during the separation phase, which can reflect the overall change trend of the TSS. The constraint condition (13) is that the libration angle is 0 at the separation ending time, which can ensure that the TSS enters a stable orbit and works normally. 2) In actual work, in order to increase the adaptability of the algorithm, (13) often becomes $|\theta_{t_f}(v,\lambda)|\le\varepsilon$, where $\varepsilon$ represents a tolerance level.

### 4.2 Algorithm to find the optimal UVDSS

Based on dynamic equations (4)–(8), it is hard to get explicit expressions of $\theta_{t_f}(v,\lambda)$ and $|\theta|_{\text{ave}}(v,\lambda)$ about $(v,\lambda)$, which makes that the frequently encountered solving algorithm can not work to solve the optimization problem (12)–(14). To resolve this dilemma, inspired by system identification theory [33–35], two back propagation (BP) neural networks are introduced to establish function models of $\theta_{t_f}(v,\lambda)$ and $|\theta|_{\text{ave}}(v,\lambda)$. Then, Newton–Raphson method of multiple initial values is used to find the zero point set of $\theta_{t_f}(v,\lambda)$. By comparing the value of $|\theta|_{\text{ave}}(v,\lambda)$ on the constraint set, $(v^*,\lambda^*)$ is obtained. The detailed process is as follows:

**Step 1** (Build the dataset of $\theta_{t_f}(v,\lambda)$ and $|\theta|_{\text{ave}}(v,\lambda)$ based on Algorithm 1)

Step 1-1: Evenly divide the sets $[\overline{v},\underline{v}]$ and $(0,L)$ with the step sizes $\Delta_1$ and $\Delta_2$ to get two sets

$$\mathcal{V}=\left\{\overline{v}+i\Delta_1\in[\overline{v},\underline{v}]|i=0,1,2,\ldots\right\}, \tag{15}$$

$$\mathcal{L}=\{i\Delta_2\in(0,L)|i=1,2,\ldots\}. \tag{16}$$

Step 1-2: For any $(v,\lambda)\in\mathcal{V}\times\mathcal{L}$, use Algorithm 1 to obtain $\theta(t;v,\lambda)$. Then, we can get

$$\Theta=\{\theta(t;v,\lambda)|(v,\lambda)\in\mathcal{V}\times\mathcal{L}\}.$$

Step 1-3: Based on $\Theta$, (10) and (11), the dataset of $\theta_{t_f}(v,\lambda)$ and $|\theta|_{\text{ave}}(v,\lambda)$ is obtained

$$\Theta_{t_f}=\{\theta_{t_f}(v,\lambda)|(v,\lambda)\in\mathcal{V}\times\mathcal{L}\},$$

$$|\Theta|_{\text{ave}}=\{|\theta|_{\text{ave}}(v,\lambda)|(v,\lambda)\in\mathcal{V}\times\mathcal{L}\}.$$

**Step 2** (Establish function models of $\theta_{t_f}(v,\lambda)$ and $|\theta|_{\text{ave}}(v,\lambda)$ based on BP neural networks, $\Theta_{t_f}$ and $|\Theta|_{\text{ave}}$)

The following takes $\theta_{t_f}(v,\lambda)$ as an example to show how to use a BP neural network to construct its function model. The one of $|\theta|_{\text{ave}}(v,\lambda)$ can be obtained similarly.

Step 2-1: Network initialization. $(v,\lambda)$ is used as the two-dimensional input vector, $\theta_{t_f}(v,\lambda)$ is the expected network output. Therefore, the number of input layer neurons is 2 and the number of output layer neurons is 1. Give the number of hidden layers and the number of corresponding neurons. Initialize each connection weight and threshold.

Step 2-2: Output calculation of the hidden layer. The hidden layer output $y_m$ is calculated as follows:

$$\begin{cases} y_1=f_1\left(w_1[\lambda\ \ v]^{\mathrm{T}}+\alpha_1\right),\\ y_2=f_2\left(w_2y_1+\alpha_2\right),\\ \vdots\\ y_m=f_m\left(w_my_{m-1}+\alpha_m\right), \end{cases}$$

where $m$ is the number of hidden layers, $w_j$ and $\alpha_j$ denote a weight matrix and a threshold vector of the $j$th hidden layer, respectively. $f_j(\cdot)$ is an activation function for the $j$th hidden layer. When $f_j(\cdot)$ acts on a vector, it means that it acts on each element of the vector and then forms a new vector.

Step 2-3: Output calculation of the output layer. The neural network output $z$ is calculated as follows:

$$z=g\left(py_m+\beta\right),$$

where $g(\cdot)$, $p$ and $\beta$ represent an activation function, a weight matrix and a threshold vector of the output layer, respectively.

Step 2-4: Error calculation. Comparing the training output $z$ with the expected output $\theta_{t_f}(v,\lambda)$, the prediction error is obtained as

$$e=\theta_{t_f}(v,\lambda)-z.$$

Step 2-5: Error backpropagation. The weights and thresholds of each layer are adjusted according to Levenberg–Marquardt algorithm [36] such that the modified network output can be close to the expected value.

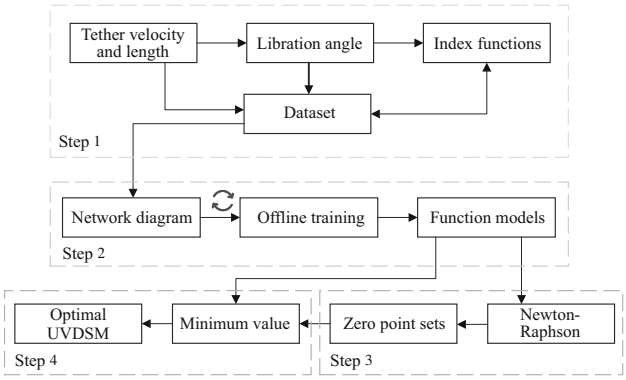


**Fig. 8** The algorithm flowchart

Step 2-6: Repeat the above process and traverse $\mathcal{V}$, $\mathcal{L}$ and $\Theta_{t_f}$ to get the function model of $\theta_{t_f}(v, \lambda)$.

**Step 3** (Find the zero point set of $\theta_{t_f}(v, \lambda)$ based on Newton–Raphson method of multiple initial values)

Based on the training function model of $\theta_{t_f}(v, \lambda)$, Newton–Raphson method of multiple initial values is used to find the zero point set of $\theta_{t_f}(v, \lambda)$. For a given $X_0 \in \mathcal{V} \times \mathcal{L}$, the iteration equation is as follows:

$$X_{k+1} = X_k - \frac{\theta_{t_f}(X_k)}{\dot{\theta}_{t_f}(X_k)}, \tag{17}$$

where $X_k = [v_k, \lambda_k]$, $k$ represents the $k$th iteration. If the limit of $X_k$ exists, then this limit can be an element of the zero point set of $\theta_{t_f}(v, \lambda)$. When $X_0$ traverses $\mathcal{V} \times \mathcal{L}$, the zero point set can be obtained as

$$\mathcal{O} = \left\{ \lim_{k \to \infty} X_k \,|\, X_0 \in \mathcal{V} \times \mathcal{L} \right\}.$$

**Step 4** (Give the optimal UVDSS $(v^*, \lambda^*)$)

Based on the training function model of $|\theta|_{\text{ave}}(v, \lambda)$, the optimal UVDSS can be obtained as

$$(v^*, \lambda^*) = \underset{(v,\lambda)\in\mathcal{O}}{\operatorname{argmin}} |\theta|_{\text{ave}}(v, \lambda).$$

The overall algorithm design is shown in Fig. 8.

***Remark 3*** Compared with the existing literature [37–39], the advantages of the method proposed by the paper can be briefly summarized in two aspects. From the research purpose point of view, the existing literature mainly discusses the properties of the UVDSS and its influence on the libration angle. The advantage of the method in this paper is that it can optimize the tether velocity and the tethers release length in the uniform velocity separation phase, and then guarantee the minimum libration angle during the release process. From the research method point of view, the advantage of the method in this paper not only takes full account of the mechanism model of the TSS, but also employs data-driven optimization techniques, that is, the method in this paper is both mechanism- and data-driven.

## 5 Numerical simulation

This section uses a numerical simulation to demonstrate the above theoretical model and analysis results. The parameters are given in Table 2. Let $\Delta_1 = 0.01$ and $\Delta_2 = 2$ in (15) and (16), which implies

$$\mathcal{V} = \{0.25 + 0.01i \in [0.25, 0.35] | i = 0, 1, 2, \ldots, 10\},$$
$$\mathcal{L} = \{2i \in (0, 800) | i = 1, 2, \ldots, 400\}.$$

### 5.1 Effectiveness of the algorithm to find the optimal UVDSS

In view of Algorithm 1, the libration angle of the entire separation process can be obtained for each UVDSS from $\mathcal{V} \times \mathcal{L}$. Then, the three-dimensional curves of $\theta_{t_f}(v, \lambda)$ and $|\theta|_{\text{ave}}(v, \lambda)$ are obtained by (11) and (10), as shown in Fig. 9a–b.

Next, we use Step 1 and Step 2 in Sect. 4.2 to establish the function models of $\theta_{t_f}(v, \lambda)$ and $|\theta|_{\text{ave}}(v, \lambda)$. The number of hidden layers is 2, and the number of neurons is 10 and 5, respectively. The activation function of the hidden layer is the tansig function, and the activation function of the output layer is the identity mapping function. The training models obtained are illustrated in (18) and (19) as follows (their curves are shown in Fig. 10a–b):

$$\theta_{t_f}(v, \lambda) = p \cdot \text{tansig}\big(w_2 \cdot \text{tansig}\big(w_1[\lambda, v]^{\mathrm{T}} + \alpha_1\big) + \alpha_2\big) + \beta, \tag{18}$$

$$|\theta|_{\text{ave}}(v, \lambda) = \bar{p} \cdot \text{tansig}\big(\bar{w}_2 \cdot \text{tansig}\big(\bar{w}_1[\lambda, v]^{\mathrm{T}} + \bar{\alpha}_1\big) + \bar{\alpha}_2\big) + \bar{\beta}, \tag{19}$$

where

$$p = \begin{bmatrix} -0.1 & -0.8 & -0.7 & 0.2 & -0.9 \end{bmatrix}, \bar{p} = \begin{bmatrix} -0.5 & -0.1 & -0.7 & 0.9 & 0.2 \end{bmatrix},$$
$$w_1 = \begin{bmatrix} -4.2 & 2.9 & 3.0 & -4.3 & -4.2 & -3.1 & 4.2 & -2.4 & 2.7 & 2.7 \\ -0.8 & -3.2 & 1.2 & -0.3 & -0.3 & -2.8 & -1.4 & -0.9 & 2.5 & -3.7 \end{bmatrix}^{\mathrm{T}}, \bar{w}_1 = \begin{bmatrix} 1.6 & -1.0 & 3.7 & 0.5 & 3.7 & -3.9 & 2.8 & 4.4 & -3.8 & 2.7 \\ 4.1 & -3.8 & 1.2 & 4.3 & -1.4 & 0.6 & 1.5 & 1.0 & -1.0 & 3.0 \end{bmatrix}^{\mathrm{T}},$$

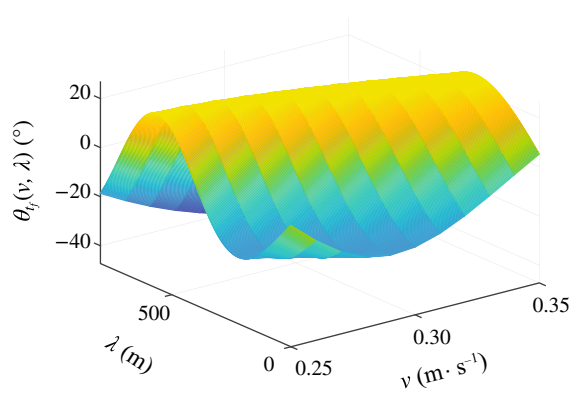


(a) The stroke plot of $\theta_{t_f}(v, \lambda)$

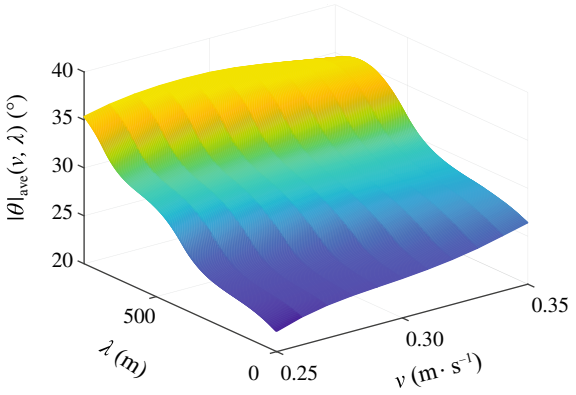


(b) The stroke plot of $|\theta|_{ave}(v, \lambda)$

**Fig. 9** The three-dimensional curves of $\theta_{t_f}(v, \lambda)$ and $|\theta|_{ave}(v, \lambda)$

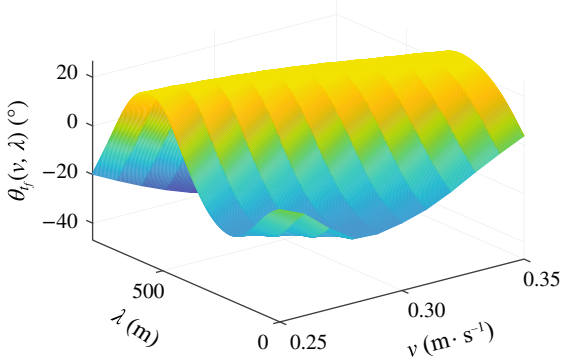


(a) The training model of $\theta_{t_f}(v, \lambda)$

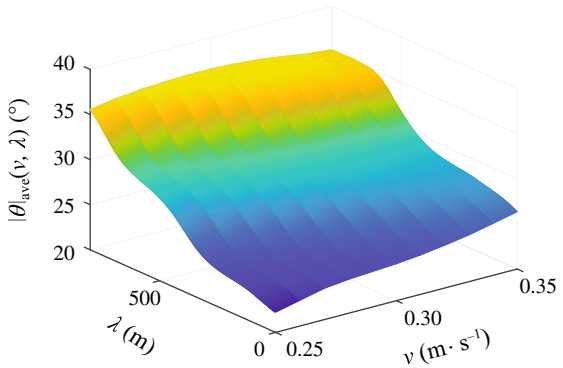


(b) The training model of $|\theta|_{ave}(v, \lambda)$

**Fig. 10** The neural network training models of $\theta_{t_f}(v, \lambda)$ and $|\theta|_{ave}(v, \lambda)$

**Table 3** The value of $|\theta|_{ave}(v, \lambda)$ with respect to $\mathcal{O}$

| $(v, \lambda)$ | $\lvert\theta\rvert_{ave}(v, \lambda)$ |
|---|---|
| (0.25 m/s, 392.67 m) | 26.76° |
| (0.26 m/s, 354.65 m) | 26.63° |
| (0.27 m/s, 315.29 m) | 26.40° |
| (0.28 m/s, 274.09 m) | 26.20° |
| (0.29 m/s, 230.38 m) | 26.03° |
| (0.30 m/s, 186.70 m) | 25.97° |
| (0.31 m/s, 145.72 m) | 26.01° |
| (0.32 m/s, 102.05 m) | 25.98° |
| (0.33 m/s, 49.99 m) | 25.80° |
| (0.34 m/s, 8.60 m) | 25.85° |

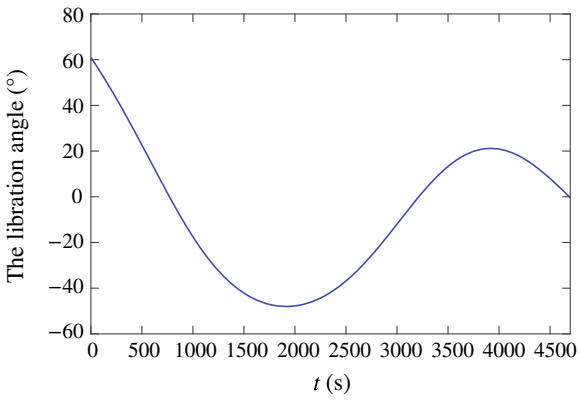


**Fig. 11** The curve of libration angle $\theta\ (t;\ v, \lambda)$

$$w_2 = \begin{bmatrix} 0.3 & 0.4 & 0.6 & 1.7 & 1.6 & 0.1 & -0.05 & 2.1 & 1.1 & -0.4 \\ -1.0 & -0.03 & 0.6 & -0.3 & -0.1 & 0.1 & 0.05 & 0.8 & -0.2 & 0.1 \\ -0.3 & -0.03 & 1.3 & -0.1 & -0.8 & 0.3 & -0.6 & 0.4 & 0.1 & -0.5 \\ 1.1 & -0.7 & -0.4 & -0.2 & -0.5 & -0.7 & -0.1 & 0.1 & 1.3 & 0.5 \\ 0.9 & -0.3 & -0.4 & -0.2 & -0.4 & 0.3 & 0.2 & -0.3 & 2.2 & -0.2 \end{bmatrix},$$

$$\bar{w}_2 = \begin{bmatrix} 0.01 & 0.3 & -0.2 & -0.4 & 0.5 & 1.0 & 0.5 & 0.7 & -0.2 & 0.5 \\ 0.2 & -0.9 & -0.5 & 0.3 & -0.4 & -0.06 & -0.1 & -0.5 & -0.6 & 0.7 \\ -0.2 & -0.07 & -0.9 & 0.04 & 0.1 & 0.2 & -0.6 & -0.1 & -0.1 & -0.2 \\ -0.8 & 0.3 & 1.0 & 0.4 & -0.07 & 0.3 & 0.03 & 0.03 & -0.3 & 0.5 \\ 0.4 & 0.2 & 0.9 & -0.2 & 0.6 & -0.3 & 0.4 & -0.7 & 0.3 & -0.8 \end{bmatrix},$$

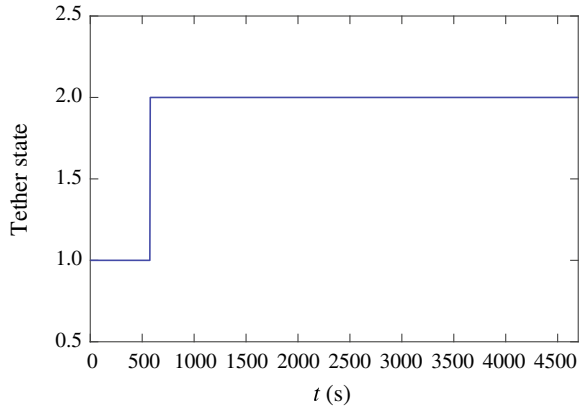


**Fig. 12** The tether state

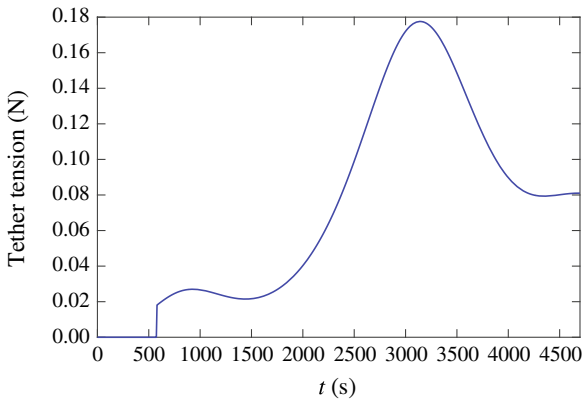


**Fig. 13** The tether tension

$$\alpha_1 = \left[4.0\ -3.8\ -1.3\ 2.6\ 0.9\ -2.0\ 1.5\ -1.2\ 3.4\ 4.1\right], \bar{\alpha}_1 = \left[-4.5\ 3.8\ -2.5\ -1.3\ -0.4\ -0.3\ 1.7\ 1.8\ -3.8\ 4.5\right],$$
$$\alpha_2 = \left[-1.7\ 2.1\ -0.4\ 1.7\ 1.9\right],\ \beta = 0.6, \bar{\alpha}_2 = \left[2.1\ 0.6\ -0.5\ 0.9\ 1.4\right],\ \bar{\beta} = -0.3.$$

By the comparison of Figs. 9a and 10a and the comparison of Figs. 9b and 10b, it can be seen that the BP neural network can model $\theta_{t_f}(v, \lambda)$ and $|\theta|_{\text{ave}}(v, \lambda)$ well.

On the basis of (18), select an element arbitrarily from $\mathcal{V} \times \mathcal{L}$ as the initial value of (17) for iterative calculation. The stop condition is set to $|X_k - X_{k-1}| \le 10^{-5}$. After the initial value traverses $\mathcal{V} \times \mathcal{L}$, the zero point set $\mathcal{O}$ is obtained as

$$\mathcal{O} = \{(0.25\ \text{m/s}, 392.67\ \text{m}), (0.26\ \text{m/s}, 354.65\ \text{m}), (0.27\ \text{m/s}, 315.29\ \text{m}), (0.28\ \text{m/s}, 274.09\ \text{m}), (0.29\ \text{m/s}, 230.38\ \text{m}), (0.30\ \text{m/s}, 186.70\ \text{m}), (0.31\ \text{m/s}, 145.72\ \text{m}), (0.32\ \text{m/s}, 102.05\ \text{m}), (0.33\ \text{m/s}, 49.99\ \text{m}), (0.34\ \text{m/s}, 8.60\ \text{m})\}.$$

By substituting each element of $\mathcal{O}$ into (19), we can obtain Table 3. It can be seen from Table 3 that when $(v, \lambda) = (0.33\ \text{m/s}, 49.99\ \text{m})$, the smallest value of $|\theta|_{\text{ave}}(v, \lambda)$ is got as 25.80°. That is, $(v^*, \lambda^*) = (0.33\ \text{m/s}, 49.99\ \text{m})$. The libration angle $\theta$ is shown in Fig. 11, the tether state is shown in Fig. 12. We find that the tether changes from a relaxation state to a stretch state at 578 s and continues until the mission is completed, where "1" indicates the tether is in the relaxation state, "2" indicates the tether is in the stretch state. In addition, the tether tension can be obtained as shown in Fig. 13.

***Remark 4*** In the simulation, there are two kinds of parameters to be selected or given, one is the parameters of the system, and the other is the parameters in the algorithm. The first kind of parameter comes from a actual system, as shown in Table 2. The second kind of parameters are obtained by training based on the available data.

## 5.2 Comparative simulation and analysis

To show the superiority of the method proposed in this paper, firstly a comparative study should be made on the BP neural network and the Newton–Raphson method.

The BP neural network method is compared with the polynomial fitting method. The root mean square error (RMSE) is used as the index to compare the fitting effect. The result is shown in Table 4. This implies that the fitting effect of the BP neural network method is better than the polynomial fitting method.

The Newton–Raphson method is compared with the binary search method. Similarly, we choose multiple values as the initial value of the iteration, and the iteration precision is set to $10^{-5}$. Then we record the number of iterations two methods require to achieve the desired accuracy for each ini-

**Table 4** RMSE of BP neural network and polynomial fitting method

| | RMSE of BP neural network | RMSE of polynomial fitting method |
|---|---|---|
| $\theta_{t_f}(v, \lambda)$ | 0.2963 | 1.6859 |
| $\lvert\theta\rvert_{\text{ave}}(v, \lambda)$ | 0.0633 | 0.3306 |

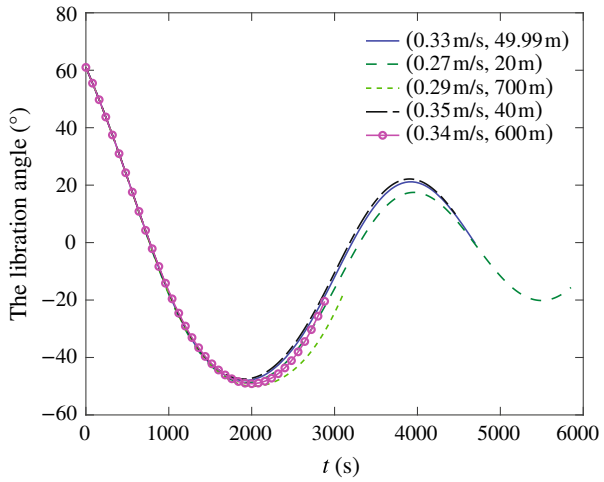


**Fig. 14** Comparison of the libration angle for five UVDSSs

**Table 5** The values of index function for five UVDSSs

| | $\theta_{t_f}(v,\lambda)$ | $\lvert\theta\rvert_{\text{ave}}(v,\lambda)$ |
|---|---|---|
| (0.33 m/s, 49.99 m) | −0.3196° | 25.8096° |
| (0.27 m/s, 20 m) | −15.6390° | 23.5232° |
| (0.29 m/s, 700 m) | −17.9755° | 35.5249° |
| (0.35 m/s, 40 m) | 9.9467° | 26.8335° |
| (0.34 m/s, 600 m) | −16.1528° | 34.4216° |

tial value. After simulation verification, the results show that, on average, the Newton iteration method requires only 4 iterations, while the binary search method requires 27 iterations. This implies that the Newton iteration method converges faster than the binary search method for the same required precision.

Next, we verify whether the UVDSS solved in this paper is the best solution. The optimal UVDSS is obtained as $(v^*, \lambda^*) = (0.33\ \text{m/s}, 49.99\ \text{m})$, and we randomly selected four UVDSSs to compare for it. Four UVDSSs are (0.27 m/s, 20 m), (0.29 m/s, 700 m), (0.35 m/s, 40 m) and (0.34 m/s, 600 m). Then we can get curves of five UVDSSs as shown in Fig. 14 and index function values corresponding to five UVDSSs as shown in Table 5. It can be seen that the optimal UVDSS solved in this paper makes the time-consuming of releasing the tether moderate and minimizes the optimality problem (12)–(14).

## 6 Conclusion

This paper has investigated the influence of the UVDSS on the motion state and the libration angle of the TSS. We have developed a numerical solution algorithm for the libration angle based on the TSS dynamics equation and Clohessy–Wiltshire equation. Furthermore, we have designed the optimization algorithm using the libration angle as the objective to obtain the optimal UVDSS. Through simulation comparison, the superiorities and advantages of the proposed method have been demonstrated.

In future work, we can consider the optimization problem with the spin angle, the tether flexibility and the satellite attitude. In addition, the optimality problem of the UVDSS is discussed in this paper, and the corresponding ideas and methods can be extended to the one of other separation schemes.

**Data Availability** The data that support the findings of this study are available upon request from the corresponding author guojin@ustb.edu.cn.

## Declarations

**Conflict of interest** The authors declare that there is no competing financial interest or personal relationship that could have appeared to influence the work reported in this paper.

## References

1. Zhu, R., Misra, A., & Modi, V. (1994). Dynamics and control of coupled orbital and librational motion of tethered satellite systems. *The Journal of the Astronautical Sciences, 42*(3), 319–342.
2. Giuseppi, A., Delli Priscoli, F., & Pietrabissa, A. (2022). Robust and fault-tolerant spacecraft attitude control based on an extended-observer design. *Control Theory and Technology, 20*, 323–337. https://doi.org/10.1007/s11768-022-00101-2
3. Haghighi, R., & Pang, C. (2016). Energy-efficient control of nanosatellites during distributed region formation flying. *Control Theory and Technology, 14*, 263–278. https://doi.org/10.1007/s11768-016-6075-9
4. Tan, S., Guo, J., Zhao, Y., & Zhang, J. (2021). Adaptive control with saturation-constrainted observations for drag-free satellites-a set-valued identification approach. *Science China Information Sciences, 64*(10), 202202. https://doi.org/10.1007/s11432-020-3145-0
5. Yang, F., Tan, S., Xue, W., Guo, J., & Zhao, Y. (2020). Extended state filtering with saturation-constrainted observations and active disturbance rejection control of position and attitude for drag-free satellites. *Acta Automatica Sinica, 46*(11), 2337–2349. https://doi.org/10.16383/j.aas.c190515
6. Hu, Y., Guo, J., Meng, W., Liu, G., & Xue, W. (2022). Longitudinal control for balloon-borne launched solar powered UAVs in near-space. *Journal of Systems Science and Complexity, 35*, 802–819. https://doi.org/10.1007/s11424-022-1302-6
7. Lu, K., Liu, H., Zeng, L., Wang, Z., Zhang, Z., & An, J. (2023). Applications and prospects of artificial intelligence in covert satellite communication: a review. *Science China Information Sciences, 66*(2), 121301. https://doi.org/10.1007/s11432-022-3566-4
8. Johnson, L., Gilchrist, B., Estes, R., & Lorenzini, E. (1999). Overview of future NASA tether applications. *Advances in Space Research, 24*(8), 1055–1063. https://doi.org/10.1016/S0273-1177(99)00553-0
9. Sanmartín, J., Martinez-Sanchez, M., & Ahedo, E. (1993). Bare wire anodes for electrodynamic tethers. *Journal of Propulsion and Power, 9*(3), 353–360. https://doi.org/10.2514/3.23629

10. Fuhrhop, K. (2007). *Theory and experimental evaluation of electrodynamic tether systems and related technologies.* Ph.D. thesis. Ann Arbor, MI, USA: University of Michigan. https://hdl.handle.net/2027.42/57663.
11. Avanzini, G., & Fedi, M. (2013). Refined dynamical analysis of multi-tethered satellite formations. *Acta Astronautica, 84*, 36–48. https://doi.org/10.1016/j.actaastro.2012.10.031
12. Colombo, G., Gaposchkin, E., Grossi, M., & Weiffenbach, G. (1975). The skyhook: A shuttle-borne tool for low-orbital-altitude research. *Meccanica, 10*, 3–20. https://doi.org/10.1007/BF02148280
13. Bilén, S., Gilchrist, B., Bonifazi, C., & Melchioni, E. (1995). Transient response of an electrodynamic tether system in the ionosphere: TSS-1 first results. *Radio Science, 30*(5), 1519–1535. https://doi.org/10.1029/95RS01889
14. Hill, M., Calhoun, R., Fernando, H., & Wieser, A. (2010). Coplanar doppler lidar retrieval of rotors from T-REX. *Journal of the Atmospheric Sciences, 67*(3), 713–729. https://doi.org/10.1175/2009JAS3016.1
15. Iki, K., Kawamoto, S., Ohkawa, Y., Okumura, T., Kawashima, K., Takai, M., Izawa, K., Matsumoto, K., Suzuki, S., Katayama, Y., Horikawa, Y., & Inoue, K. (2016). Expected on-orbit tether deployment dynamics on the KITE mission. *Transactions of the Japan Society for Aeronautical and Space Sciences, Aerospace Technology Japan, 14*(30), 9–18. https://doi.org/10.2322/tastj.14.Pr_9
16. Cartmell, M., & Mckenzie, D. (2008). A review of space tether research. *Progress in Aerospace Sciences, 44*(1), 1–21. https://doi.org/10.1016/j.paerosci.2007.08.002
17. Chen, Y., Huang, R., He, L., Ren, X., & Zheng, B. (2014). Dynamical modelling and control of space tethers: a review of space tether research. *Nonlinear Dynamics, 77*(4), 1077–1099. https://doi.org/10.1007/s11071-014-1390-5
18. Beletskii, V., & Pivovarov, M. (2000). The effect of the atmosphere on the attitude motion of a dumb-bell-shaped artificial satellite. *Journal of Applied Mathematics and Mechanics, 64*(5), 691–700. https://doi.org/10.1016/S0021-8928(00)00097-6
19. Burov, A., & Kosenko, I. (2015). Planar oscillations of a dumbbell of a variable length in a central field of Newtonian attraction. exact approach. *International Journal of Non-Linear Mechanics, 72*, 1–5. https://doi.org/10.1016/j.ijnonlinmec.2015.01.011
20. Yu, B., Dai, P., & Jin, D. (2018). Modeling and dynamics of a bare tape-shaped tethered satellite system. *Aerospace Science and Technology, 79*, 288–296. https://doi.org/10.1016/j.ast.2018.05.046
21. Liu, C., Chen, S., Guo, Y., & Wang, W. (2023). Robust adaptive control for rotational deployment of an underactuated tethered satellite system. *Acta Astronautica, 203*, 65–77. https://doi.org/10.1016/j.actaastro.2022.11.025
22. Chu, Z., Di, J., & Cui, J. (2018). Hybrid tension control method for tethered satellite systems during large tumbling space debris removal. *Acta Astronautica, 152*, 611–623. https://doi.org/10.1016/j.actaastro.2018.09.016
23. Bourabah, D., & Botta, E. (2022). Length-rate control for libration reduction during retraction of tethered satellite systems. *Acta Astronautica, 201*, 152–163. https://doi.org/10.1016/j.actaastro.2022.08.037
24. Su, B., Zhang, F., & Huang, P. (2021). Robust control of triangular tethered satellite formation with unmeasured velocities. *Acta Astronautica, 186*, 190–202. https://doi.org/10.1016/j.actaastro.2021.04.045
25. Shan, M., & Shi, L. (2022). Velocity-based detumbling strategy for a post-capture tethered net system. *Advances in Space Research, 70*(5), 1336–1350. https://doi.org/10.1016/j.asr.2022.06.012
26. Vadali, S. (1991). Feedback tether deployment and retrieval. *Journal of Guidance, Control, and Dynamics, 14*(2), 469–470. https://doi.org/10.2514/3.20662
27. Wen, H., Zhu, Z., Jin, D., & Hu, H. (2016). Space tether deployment control with explicit tension constraint and saturation function. *Journal of Guidance, Control, and Dynamics, 39*(4), 916–921. https://doi.org/10.2514/1.G001356
28. Fujii, H., & Ishijima, S. (1989). Mission function control for deployment and retrieval of a subsatellite. *Journal of Guidance, Control and Dynamics, 12*(2), 243–247. https://doi.org/10.2514/3.20397
29. Li, X., Sun, G., Han, S., & Shao, X. (2021). Fractional-order nonsingular terminal sliding mode tension control for the deployment of space tethered satellite. *IEEE Transactions on Aerospace and Electronic Systems, 57*(5), 2759–2770. https://doi.org/10.1109/TAES.2021.3061815
30. Clohessy, W., & Wiltshire, R. (1960). Terminal guidance system for satellite rendezvous. *Journal of the Aerospace Science, 27*, 653–674. https://doi.org/10.2514/8.8704
31. Tan, D., & Chen, Z. (2012). On a general formula of fourth order Runge–Kutta method. *Journal of Mathematical Science and Mathematics Education, 7*(2), 1–10.
32. Butcher, J. (1996). A history of Runge–Kutta methods. *Applied Numerical Mathematics, 20*(3), 247–260. https://doi.org/10.1016/0168-9274(95)00108-5
33. Guo, J., Jia, R., Su, R., & Zhao, Y. (2023). Identification of fir systems with binary-valued observations against data tampering attacks. *IEEE Transactions on Systems, Man, and Cybernetics: Systems, 53*(9), 5861–5873. https://doi.org/10.1109/TSMC.2023.3276352
34. Guo, J., & Diao, J. (2020). Prediction-based event-triggered identification of quantized input fir systems with quantized output observations. *Science China Information Sciences, 63*, 112201–111220112. https://doi.org/10.1007/s11432-018-9845-6
35. Guo, J., Wang, X., Xue, W., & Zhao, Y. (2021). System identification with binary-valued observations under data tampering attacks. *IEEE Transactions on Automatic Control, 66*(8), 3825–3832. https://doi.org/10.1109/TAC.2020.3029325
36. Xie, Y., & Ma, C. (2011). A smoothing Levenberg–Marquardt algorithm for solving a class of stochastic linear complementarity problem. *Applied Mathematics and Computation, 217*(9), 4459–4472. https://doi.org/10.1016/j.amc.2010.10.049
37. Zhang, Y., Jiang, X., Bai, Z., Guo, J., & Wei, C. (2022). Dynamics and rebound behavior analysis of flexible tethered satellite system in deployment and station-keeping phases. *Defence Technology, 18*(3), 509–523. https://doi.org/10.1016/j.dt.2021.04.007
38. Luo, L., Li, A., & Wang, C. (2014). Simulation analysis of orbital parameters of small satellite launching by space tether system. In: *Proceedings of the 33rd Chinese Control Conference*, pp. 6398–6402. https://doi.org/10.1109/ChiCC.2014.6896042.
39. Ji, Z., & Shi, G. (2023). Adaptive neural dynamics-based speed control strategy for stable retrieval of tethered satellite system. *Advances in Space Research, 71*(12), 4987–4994. https://doi.org/10.1016/j.asr.2023.01.061

**Peng Yu** received the B.Sc. degree from Hebei University of Science and Technology, Hebei, China, in 2018 and the M.Sc. degree from Yanshan University, Hebei, China, in 2021. He is currently working toward the Ph.D. degree majoring in control system theory at the School of Automation and Electrical Engineering, University of Science and Technology Beijing, Beijing, China. His research interests include the control of tethered satellite systems and security control of cyber physical systems.

**Ji-Feng Zhang** received the B.Sc. degree in mathematics from Shandong University, China, in 1985 and the Ph.D. degree from the Institute of Systems Science (ISS), Chinese Academy of Sciences (CAS), China, in 1991. He is now with the ISS, Academy of Mathematics and Systems Science, CAS. His current research interests include system modeling, adaptive control, stochastic systems, and multi-agent systems. He is a Fellow of IEEE, IFAC, CAA and CSIAM, member of the European Academy of Sciences and Arts, and Academician of the International Academy for Systems and Cybernetic Sciences. He received the Second Prize of the State Natural Science Award of China in 2010 and 2015, respectively. He was the director of the Institute of Systems Science, Academy of Mathematics and Systems Science, Chinese Academy of Sciences; a Vice-President of the Chinese Association of Automation, the Chinese Mathematical Society, and the Systems Engineering Society of China; a Vice-Chair of the IFAC Technical Board, member of the Board of Governors, IEEE Control Systems Society; Convenor of Systems Science Discipline, Academic Degree Committee of the State Council of China. He has served as Editor-in-Chief, Deputy Editor-in-Chief, Senior Editor or Associate Editor for more than 10 journals, including *Science China Information Sciences*, *National Science Review*, *IEEE Transactions on Automatic Control*, and *SIAM Journal on Control and Optimization* etc.

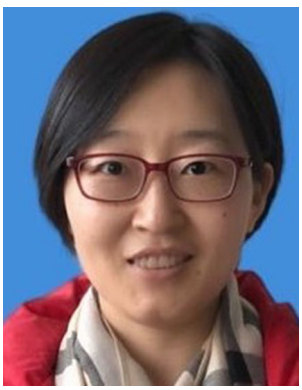

**Shuping Tan** received the B.Sc. degree in mathematics from Shandong University, Jinan, China, in 2001, and the Ph.D. degree in control theory from the Academy of Mathematics and Systems Science, Chinese Academy of Sciences, Beijing, China, in 2006. She is currently a professor in Beijing Institute of Control Engineering. Her current research interests include tethered satellite system control and drag-free control.

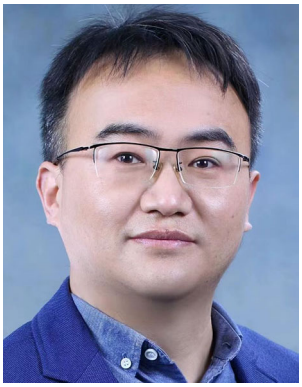

**Jin Guo** received the B.Sc. degree in mathematics from Shandong University, Jinan, China, in 2008, and the Ph.D. degree in system modeling and control theory from the Academy of Mathematics and Systems Science, Chinese Academy of Sciences, Beijing, China, in 2013. He is currently a Professor with the School of Automation and Electrical Engineering, University of Science and Technology Beijing, Beijing. His research interests are system modeling and identification, adaptive control, and systems biology. Prof. Guo is an Associate Editor of *Asian Journal of Control* and *Journal of Systems Science and Complexity*.

**Yanlong Zhao** received the B.Sc. degree in mathematics from Shandong University, Jinan, China, in 2002, and the Ph.D. degree in systems theory from the Academy of Mathematics and Systems Science, Chinese Academy of Sciences, Beijing, China, in 2007. Since 2007, he has been with the AMSS, CAS, where he is currently a Professor. His research interests include identification and control of quantized systems, and modeling of communication systems, etc. He served as Vice President of Asian Control Association and Vice President of IEEE CSS Beijing Chapter, and is now Vice General Secretary of Chinese Association of Automation (CAA), Chair of Technical Committee on Control Theory (TCCT), CAA. He has been a Deputy Editor-in-Chief of the *Journal of Systems and Science and Complexity*, an Associate Editor of *Automatica*, *SIAM Journal on Control and Optimization* and *IEEE Transactions on Systems, Man and Cybernetics*; and was the Editor of the *IFAC Symposium on System Identification* in 2015.